THERMAL CREEP EFFECTS IN ISOTHERMAL WALL MICROCHANNELS

H. Niazmand[1], A. Amiri Jaghargh[1], M. Renksizbulut[2]

[1] *Ferdowsi University of Mashhad, Mechanical Engineering Department, Mashhad, Iran*
[2] *University of Waterloo, Mechanical & Mechatronics Engineering Department, Waterloo, Ontario, Canada, N2L 3G1*

ABSTRACT

In the present work the effects of thermal creep on the development of fluid flow and heat transfer in rectangular microchannels with constant wall temperature in the slip flow regime, $10^{-3} \le Kn \le 10^{-1}$, is investigated. To avoid the unrealistically large axial temperature gradients due to the upstream axial conduction associate with low Re flows in microchannels and the uniform inlet temperature, an adiabatic section is considered at the inlet of the constant wall temperature channel. Navier-Stokes and energy equations are solved numerically using a control volume technique, while velocity slip and temperature jump conditions are applied at walls. Despite the constant wall temperature, axial temperature gradients form in the gas layer adjacent to the wall due to the temperature jump condition. Thermal creep effects due to the axial temperature gradients that are considerable in the early sections of the channel affect the flow and temperature fields especially at low Reynolds numbers flows. The effects of slip and thermal creep on the flow patterns and key flow parameters are examined in detail for a wide range of cross sectional aspect ratios, Knudsen and Reynolds numbers.

INTRODUCTION

Micro scale devices including sensors, actuators, heat exchangers, and micro power systems among others require gaseous flow through microchannels, where the typical length scale are measured in microns. For such devices the channel dimensions become comparable to the mean free path of the gas molecules even at normal pressure condition and gas flow is associated with some degrees of rarefaction effects. The Knudsen number, which is defined as the ratio of gas mean free path to the appropriate length scale of the system, is a proper parameter to measure this effect. Flow with Knudsen number in the range of $10^{-3} \le Kn \le 10^{-1}$, relevant to most microchannel applications, is called slip-flow regime. Despite the breakdown of the continuum assumption in a thin layer adjacent to the wall of microchannels, experimental evidence (Wu and Little, 1983, Beskok and Karniadakis, 1992, and turner et al, 2004) strongly supports the applicability of Navier-Stokes equation with modified boundary conditions in the slip flow regime. Basically, it is assumed that the velocity and temperature of the fluid adjacent to the wall are finitely deferent from those of the wall due to the non-continuum effects known as velocity slip and temperature jump conditions. Based on a momentum and an energy balance near the wall it can be shown that the velocity-slip and temperature-jump at the walls are proportional to their normal gradients at the wall.

Besides the transverse velocity gradients, there is another contribution to the velocity slip due to the tangential temperature gradient along the gas layer adjacent to the wall known as the thermal creep effect. It is important to note that this effect is related to the existence of axial temperature gradients in the gas layers adjacent to the wall and thus can occur even for constant wall temperature microchannels due to the temperature jump condition applied in the slip regime. For low Reynolds number flows associated with microfluidic devices thermal creep can affect the flow and thermal fields significantly, when accompanied by sufficient axial temperature gradients.

A survey of available literatures indicates a limited number of studies on the effect of thermal creep in microchannels. Rij et al. (2007) numerically studied fluid flow and heat transfer in the entrance region of a planar microchannel. Both thermally and hydrodynamically developing slip flows with prescribed constant creep velocities were investigated. They also presented an analytical solution for fully developed flow. Chen and Weng (2006) numerically analyzed the developing natural convection with thermal creep in a vertical isothermal microchannel. It was found that thermal creep increases the flow rates, reduces the drag, and enhances the heat transfer rates. In their more recent study (2008) a constant wall heat flux microchannel was considered and similar findings were reported. Sazhin et al. (2008) studied the thermal creep phenomenon through straight cylindrical capillaries in the free molecular flow regime using the DSMC method. Méolans and Graur (2008) developed an analytical model for thermal creep flow. They considered a planar microchannel between two reservoirs maintained at the same pressure, while a constant temperature gradient was applied along the channel. Bao and Lin (2008) used the Burnett equations with slip boundary conditions to model the compressible gas flow and heat transfer in micro Poiseuille flow in slip and transition flow regimes. The thermal creep contribution on the slip velocity was taken into consideration in the simulation. They concluded that thermal creep only affects the velocity slip at the entrance region, where high tangential temperature gradients occur. An analytical solution for the velocity profile of the compressible Poiseuille flow with constant heat flux boundary condition considering the thermal creep effect is derived by Ghahremani et al. (2008). Using a perturbation method, they concluded that the thermal creep increases the velocity and the flow rate for a heating case. It was also shown that this effect is only considerable for low orders of magnitude of the Brinkman number (as low as 10^{-2}).

This brief review reveals that analytical studies related to thermal creep effects are usually restricted to

the fully developed conditions and simplified geometries, while in numerical calculations thermal creep has been studied either assuming constant temperature gradient at wall or prescribed creep velocity. Therefore, there is a need for further studies to identify the thermal creep effects in cases where these simplified assumptions are not employed.

In the present study, incompressible gaseous slip-flows and heat transfer in the entrance region of rectangular microchannels are investigated for a constant wall temperature condition. Three-dimensional Navier-Stokes and energy equations along with velocity-slip and temperature-jump boundary conditions are solved numerically by a control-volume method. The effects of thermal creep and axial heat conduction are included in the analysis. Flow fields, temperature patterns, friction and heat transfer coefficients are examined in detail for a wide range of Reynolds numbers, $0.1 \le Re \le 5$, aspect ratios, $0.2 \le \alpha^* \le 1$, and Knudsen numbers, $Kn \le 0.1$.

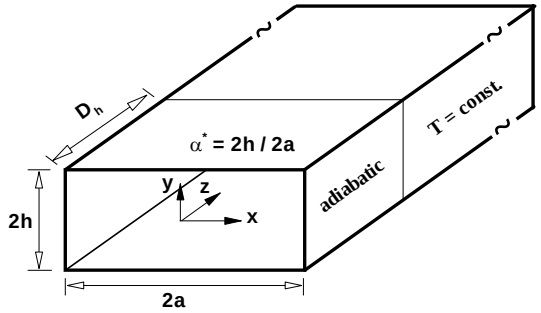

Figure 1. Schematic of flow geometry

MATHEMATICAL MODEL

The flow geometry and the coordinate system are shown in Figure 1. In the present problem, the axial temperature gradient of gas layer adjacent to wall is important in the evaluation of thermal creep, which is not well defined just at the inlet due to the applied boundary conditions. To avoid this problem an adiabatic wall has been considered at the inlet extended to one hydraulic diameter. Thereafter, the constant wall temperature is applied. In this way, unrealistically large axial temperature gradients will be avoided when the gas enters the constant wall temperature region due to the upstream axial conduction which is important in microchannel flows.

The Reynolds and the Knudsen numbers are the governing parameters in this problem and are defined as $Re = \rho W_i D_h / \mu$ and $Kn = \lambda / D_h$, where W_i , D_h and λ are the inlet velocity, hydraulic diameter and gas mean free path, respectively. Mean free path is evaluated based on the inlet conditions according to:

$$\lambda = \frac{\mu}{\rho\sqrt{2RT/\pi}} \tag{1}$$

where R is the specific gas constant taken as R = 287 J/Kg.K for all cases. For a given Knudsen number the hydraulic diameter is calculated from $D_h = \lambda /$ Kn, and the channel dimensions are then calculated based on the given channel aspect ratio, α^* = 2h / 2a, and definition of hydraulic diameter as $D_h = 4(ah)/(a+h)$.

Laminar flow is considered with negligible compressibility effects in the limit of low Mach number flows. For constant thermophysical properties, the governing equations including continuity, momentum and energy equations are as follows:

$$\int_A \rho\vec{V}\cdot d\vec{A} = 0 \tag{2}$$

$$\frac{\partial}{\partial t}\int_\forall \rho\vec{V}d\forall + \int_\forall \rho\vec{V}\cdot\vec{\nabla}\vec{V}\,d\forall = -\int_A p d\vec{A} + \int_A \mu\vec{\nabla}\vec{V}\cdot d\vec{A} \tag{3}$$

$$\frac{\partial}{\partial t}\int_\forall \rho C_p T d\forall + \int_\forall \rho C_p\vec{V}\cdot\vec{\nabla}T d\forall = \int_A k\vec{\nabla}T\cdot d\vec{A} \tag{4}$$

where $\vec{V}$, T, ρ, p, μ, c_p and k are the velocity vector, temperature, density, pressure, dynamic viscosity, specific heat and thermal conductivity, respectively. The convective terms in momentum and energy equations are transformed into volume integrals (non-conservative form) in order to limit the errors than can propagate due to the sensitivity of the continuity equation at low Mach number flows.

Boundary Conditions

Inflow boundary conditions correspond to uniform flat profiles such that $w = w_i = w_m$ and $T = T_i$ where subscripts i and m refer to inlet and mean bulk condition, respectively. The inlet velocity is obtained from Reynolds number while the inlet temperature T_i = 300K is applied in all cases. Fully developed conditions with zero gradients are assumed at the outlet, while the pressure is set to zero. At all other boundaries including the inlet, zero pressure gradients are applied. The flow satisfies the well known velocity-slip and temperature-jump boundary conditions at the walls as:

$$w_s = \left(\frac{2-\sigma_v}{\sigma_v}\right)\lambda\left(\frac{\partial w}{\partial n}\right)_g + \frac{3}{4}\frac{\mu}{\rho T_g}\left(\frac{\partial T}{\partial s}\right)_g \tag{5}$$

$$T_g - T_w = \left(\frac{2-\sigma_T}{\sigma_T}\right)\left(\frac{2\gamma}{\gamma+1}\right)\frac{\lambda}{\mathrm{Pr}}\left(\frac{\partial T}{\partial n}\right)_g \tag{6}$$

The other velocity components are specified similarly. Here, w_s is slip velocity defined as $w_s = w_g - w_w$ which is the difference between solid wall velocity, w_w, and velocity of the gas adjacent to the wall, w_g. The subscript w identifies a wall with a normal coordinate n and tangential coordinate s. The subscript g indicates the first layer of the gas adjacent to the wall where the normal and tangential gradients are evaluated. The coefficients σ_v and σ_T, known as the tangential-momentum and energy accommodation coefficients, are usually determined experimentally. For many engineering applications they are close to one and are taken as unity for simplicity. The last term in equation 5 is known as thermal creep, which implies that tangential temperature gradient at wall can introduce a fluid flow in the absence of any other deriving forces in the direction of cold to hot. It must be emphasized that thermal creep is only considered in the axial direction. The wall

temperature and Prandtl number are set to T_w = 350K and Pr = 1, respectively for all cases considered.

NUMERICAL MODEL

The numerical solution is based on a projection-type method which solves the flow field in two steps. First, an intermediate velocity field is obtained using the available pressure field. Next, velocity and pressure corrections are calculated from a Poison equation designed to satisfy the continuity equation. The numerical scheme was originally developed by Chorin (1968), and improved further by Dwyer (1989) and the present authors (Niazmand et al., 2008). Also, a pressure correction based on the conservation of cross sectional mass flux is introduced, which greatly enhances the convergence rate of the numerical scheme. A pressure defect for a given cross section is associated with the average velocity defect $\Delta w'$ at the same cross section according to the following equation:

$$\rho \frac{\Delta w'}{\Delta t} = -\frac{\partial p'}{\partial z} \tag{7}$$

The average velocity defect is defined as $\Delta w' = \overline{W} - W_i$ where $\overline{W}$ is the predicted cross sectional averaged velocity. Thus, the pressure filed is updated through the above correction and then the new velocity field is obtained using the updated pressure field.

The details of the grid independence studies, as well as evidence of accuracy in predicting the microchannel flow features are given elsewhere (Renksizbulut et al., 2006, Niazmand et al., 2008, 2009) and therefore, will not be repeated here. For most cases considered here a mesh of 51×51×141 grid points in *x, y* and *z* directions with expansion ratios of 1.06, 1.1 and 1.015, respectively has been used.

RESULTS AND DISCUSSION

Thermophysical properties of air at the inlet temperature have been used in all calculations; however, the thermal conductivity has been adjusted such that the Prandtl number becomes one. Pr = 1 has the advantage that the non-dimensional length for both momentum, $z^+ = z/(D_h\mathrm{Re})$, and energy equations, $z^* = z/(D_h\mathrm{PrRe})$, has identical values corresponding to same physical axial location. The Reynolds numbers are chosen in the range of 0.1 ≤ Re ≤ 5, related to microchannel applications and the incompressibility condition, which limits the Reynolds number severely in the slip flow regime. The effects of slip, thermal creep, and temperature jump have been examined on the flow and thermal fields and on the friction and heat transfer coefficients.

Velocity Field

As mentioned earlier, a small adiabatic section has been added to the channel inlet to properly simulate the physics of the problem. Note that constant inlet temperature condition is physically valid when the axial conduction is smaller than convective effects. For low Peclet number (Pe = RePr) flows as is the case with microchannel gas flows, axial diffusion is in the order of convection or even more dominant for cases with Pe<1. Therefore, constant inlet temperature is physically inappropriate for such flows since the upstream axial conduction can change the inlet temperature. Enforcing this condition leads to nonphysical high axial gradients, which reflects as large thermal creep effects. The adiabatic entrance section, which extends for one D_h may resemble a reservoir in the actual cases that allows the inlet of the constant wall temperature section to become part of the solution domain, where upstream axial conduction reflects in its cross sectional temperature distribution. It is worth mentioning that specifying uniform velocity at the inlet of the microchannels is less problematic as compared to uniform inlet temperature, since velocity slip at the wall, which is fairly large at the inlet due to the large velocity gradients leads to almost uniform flat velocity profiles in the early sections of the channel as will be discussed later.

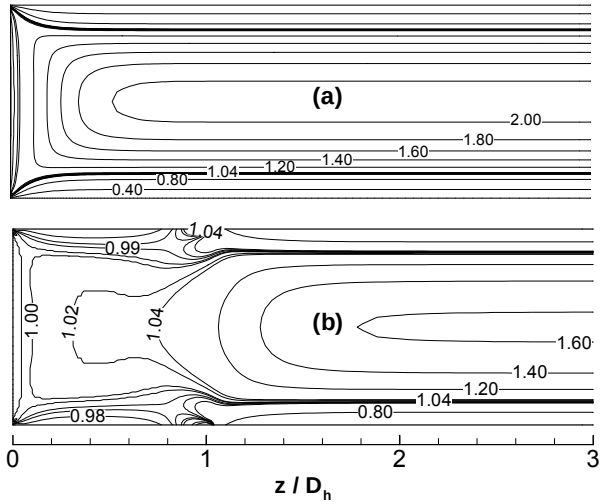

Figures 2a-b. Comparison of axial velocity field at Re=0.1, (a) Kn = 0, (b) Kn = 0.1

To gain a global view of the slip effects on the flow development, the axial velocity contours have been plotted in the symmetry plane of a square microchannel for Re = 0.1 in Figures 2a-b. Figure 2a corresponds to the no-slip condition, Kn = 0, while in Figure 2b slip condition is applied, Kn =0.1. Velocity contours for the case with slip indicate that inlet velocity profile remains almost unchanged along the adiabatic section corresponding to full slip at the wall. However, as flow passes along the constant wall temperature section the thermal creep contribution to the velocity slip vanishes, yet a considerable velocity slip exists at the wall due to the normal velocity gradients. Comparing Figure 2a with 2b, the flat velocity profile for the slip case with much smaller core velocity as compared to the no slip case is apparent. More details about the velocity development in the slip flow regime can be obtained from Figure 3 where the three dimensional axial velocity profiles are shown for the same conditions as those in Figure 2b. Clearly, in the adiabatic section, z^+ = 0.21 up to 7.63, the axial velocity profiles remain almost flat. However, close to the constant wall temperature section, where the axial temperature gradients become large, the thermal creep contribution to the slip velocity approaches

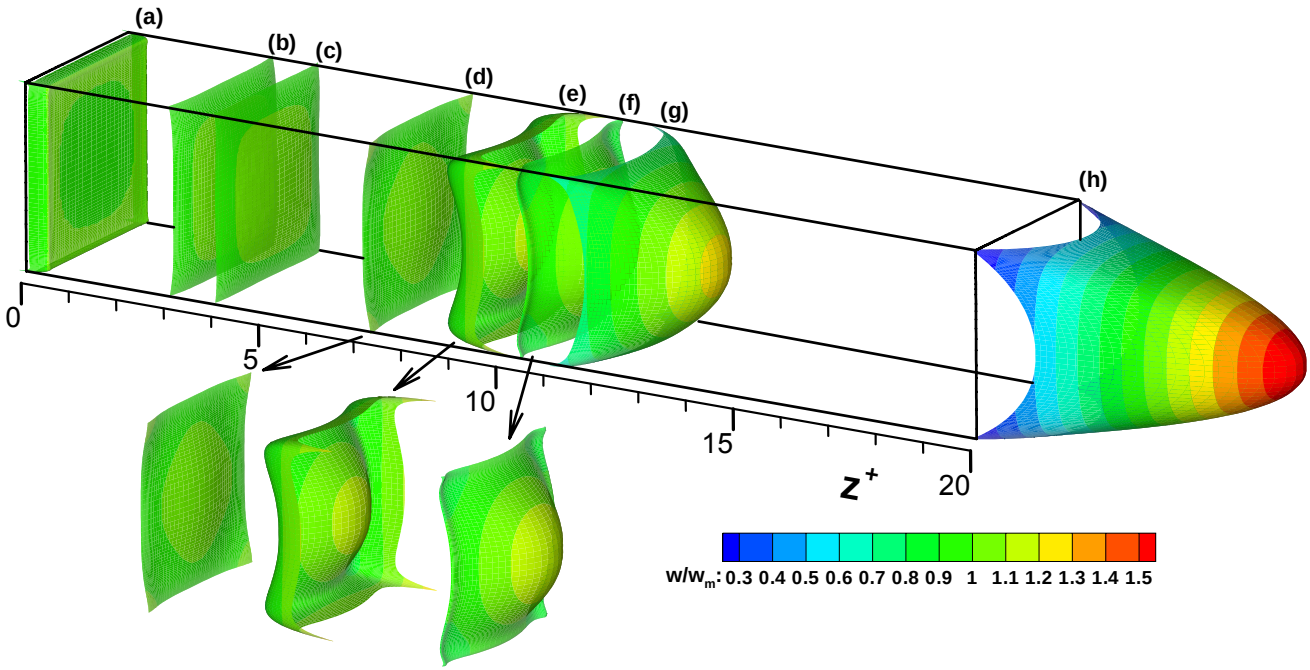

Figure 3. Variations of velocity profile along a square channel for Re = 0.1 and Kn = 0.1 at some selected axial locations, z^+ = 0.21, 3.85, 5.59, 7.63, 10, 10.51, 11.32 and 20.

its maximum value as shown in Figure 4, and therefore, there is a local maximum velocity at the channel walls and specially in the coroners where high axial temperature gradients exist.

Figure 4 shows the axial variation of the peripherally averaged velocity slip normalized by the cross sectional averaged axial velocity. The contributions of the normal velocity gradients and axial temperature gradients to the velocity slip are also shown. Figure shows, around the axial location of z^+ = 10, where the constant wall temperature section begins, the normal velocity gradient contribution becomes negative, which means that this contribution opposes the velocity slip imposed by the axial temperature gradients, which is maximum right at this location. Clearly, thermal creep is the only source for velocity overshoots observed at the walls in cross section (e) in Figure 3. Note that the axial velocity profiles for three cross sections around z^+ = 10 are shown separately in Figure 3 for more clarity.

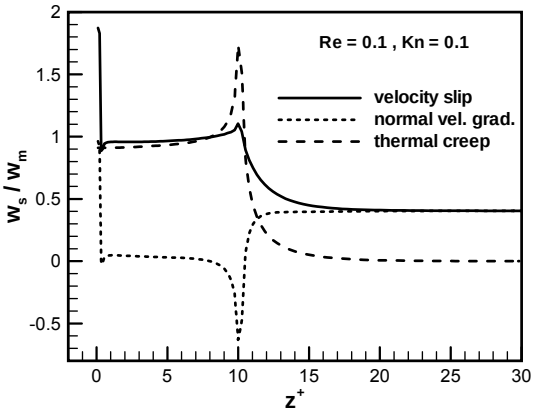

Figure 4. Axial variation of velocity slip and its contributions in a square microchannel at Re = 0.1 and Kn = 0.1.

Thermal creep contribution to the velocity slip vanishes rather fast in the early sections of the constant wall temperature since the tangential temperature gradients close to the wall approaches zero, while normal velocity gradients contribution gains weight (see Figure 4), yet the velocity overshoots at the wall reduce dramatically as the velocity profile at cross section (f) in Figure 3, z^+ = 10.51, indicates. As flow advances to the axial location of z^+ = 11.32, where both contributions to the velocity slip are equal (Figure 4), no trace of the velocity overshoots can be observed and the velocity profile shows almost the fully developed structure (z^+ = 20) with a parabolic slip velocity distribution at the wall with the minimum slip velocities occurring in the corners due to lower velocity gradients there.

For a given geometry velocity slip is directly related to the Reynolds and Knudsen numbers. In the presence of thermal creep velocity slip becomes more pronounced as Reynolds number decreases and the Knudsen increases. Clearly, slip effects are stronger at higher Knudsen numbers; however, at constant inlet and wall temperatures, with increasing Reynolds number the normal velocity gradients increase, while thermal creep effect decreases. Since in the adiabatic section the thermal creep contribution to the velocity slip is dominant, the net effect is a reduction in velocity slip as shown in Figure 5. In this figure, the axial variations of the normalized peripherally averaged velocity slip are plotted for Kn = 0.1 and different Reynolds numbers for a square microchannel. In the same figure, the contribution of normal velocity gradients and thermal creep are plotted. However, thermal creep effects are plotted separately in the upright corner for more clarity. Clearly, larger Re increase the cross sectional average velocity and at the same time increase the heat transfer rate, which increases the temperature of the gas layer in the

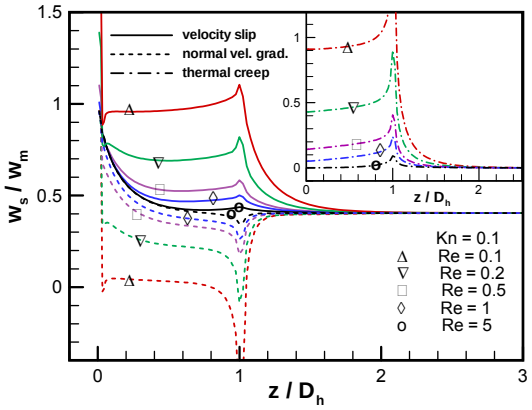

Figure 5. Effects of Re number on velocity slip and its contribution for a square microchannel at Kn = 0.1.

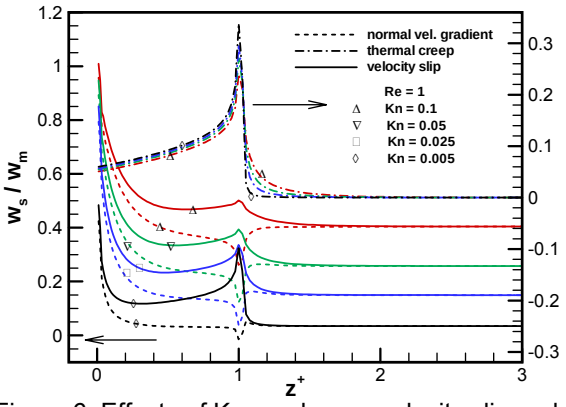

Figure 6. Effects of Kn number on velocity slip and its contributions for a square microchannel at Re = 1.

immediate vicinity of the wall, where both effects reduce the thermal creep contribution to the velocity slip. In contrast, the normal gradient contribution to the slip increases directly with the increase in Reynolds number. More details about the contributions of each component to slip velocity will be given in connection with Figure 11.

Note that except for Re = 0.1 where the contribution of the normal velocity gradients becomes negative close to z / D_h = 1, for all other Re, despite the major reduction of this contribution to the velocity slip in this region, its contribution remains positive. As mentioned earlier, the spike in the velocity slip at z / D_h = 1 is related to the strong axial temperature gradients that exist there. Also note that in the fully developed region the slip velocity is almost independent of Re number.

Similar to Figure 5, the axial variation of the normalized peripherally averaged velocity slip is plotted in Figure 6 for a fixed Re = 1 and varying Kn. Again a square microchannel is considered and the contributions of both components are shown. As indicated by equation 5, normal velocity gradient contribution to the velocity slip is directly related to Kn, and therefore, increases with increasing Kn. However, thermal creep effects are not directly influenced by the Knudsen number. Yet, since velocity field is affected by the slip due to the normal velocity gradient, which then reflects in thermal field, thermal creep effects slightly increase with an increase in Kn. Note that thermal creep dependence on Kn is much weaker than normal velocity gradient contribution. Therefore, as shown in Figure 6, thermal creep effects are more pronounced at lower Knudsen numbers, where normal velocity gradient contribution is weaker.

From both Figures 5 and 6, it can be observed that in the constant wall temperature section, where tangential temperature gradients are only due to the temperature jump condition, thermal creep effects vanishes as Kn approaches the continuum limit.

To study the pressure drop along the channel it is customary to use an apparent friction coefficient which is basically the non-dimensional form of the pressure drop defined as:

$$f_{app}\,\mathrm{Re} = \frac{1}{4z^+}\frac{\Delta\bar{p}}{\rho W_i^2/2} \qquad (8)$$

where $\Delta\bar{p}$ indicates pressure drop from the inlet. In addition to the wall shear stresses, which are the only sources of the pressure drop in fully developed region, changes in the momentum rate account for the major portion of the pressure drop in the entrance region.

Variations of apparent friction coefficient along a square microchannel at Re = 1 for different Kn numbers are shown in Figure 7.

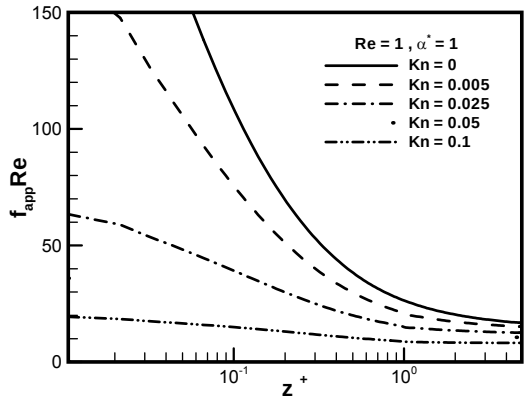

Figure 7. Axial variations of apparent friction coefficients in a square microchannel at Re = 1.

Major reduction in the apparent friction coefficient in the entrance region can be attributed to two factors. Slip reduces the wall shear stresses and at the same time less pressure drop is required for transforming the velocity profile from uniform inlet profile to the fully developed profile (since fully developed velocity profiles are much flatter as compared to those with the no-slip condition). These two factors result in lower friction coefficients at higher Kn numbers. Both factors are slightly enhanced when the contribution of thermal creep is considered. The change of fully developed *f*Re for variation of Kn number from 0.0 to 0.1 at Re = 1 is about 43% in a square microchannel, while this value increases to about 50% for a channel with aspect ratio of 0.2.

Despite the presence of a spike in the velocity slip at z / D_h = 1, the apparent friction coefficients in Figure 7 vary monotonically at all Knudsen numbers. This is true for Re = 1, however, at lower Reynolds numbers, where thermal creep effects are more influential a valley appears at the same location in the axial

variation of the apparent friction coefficients as shown in Figure 8. In this figure the axial variations of apparent friction coefficients are plotted for a square channel at Kn = 0.1 and different Reynolds numbers.

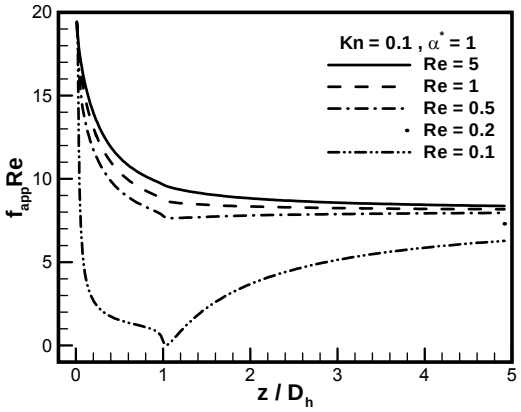

Figure 8. Effects of Re number on the axial variations of apparent friction coefficients in a square microchannel at Kn = 0.1.

Although the apparent friction coefficients vary with Re number it should be noted that their fully developed values are independent of Re number (Figure 8 does not include the fully developed region).

Geometry effects on the fully developed values of friction coefficient are shown in Figure 9. At Re = 0.1 and for several Knudsen numbers, fully developed friction coefficients are plotted as a function of aspect ratio. Pressure drop associated with narrower channels are higher, while velocity slip, which increases with increasing Knudsen number decreases the friction coefficients dramatically particularly at lower aspect ratios.

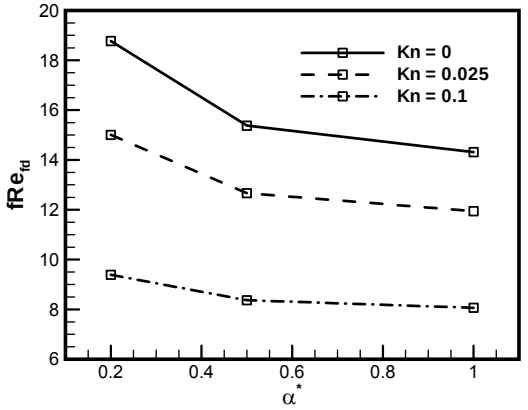

Figure 9. Fully developed friction coefficients as a function of aspect ratio for various Kn numbers.

Temperature Field

Dimensionless temperature for a constant wall temperature flow may be defined as:

$$\theta = \frac{T - T_i}{T_w - T_i} \tag{9}$$

where T_i and T_w are inlet temperature and constant wall temperature, respectively. As mentioned earlier, despite the constant wall temperature, the gas temperature adjacent to the wall can vary both peripherallyly and axially due to the temperature jump condition. Therefore, the peripherally averaged gas temperature is defined as:

$$T_g = \frac{1}{P}\int T_{g,l}\, ds \tag{10}$$

where P, $T_{g,l}$ and ds are the channel perimeter, local gas temperature adjacent to the wall and peripheral differential element, respectively.

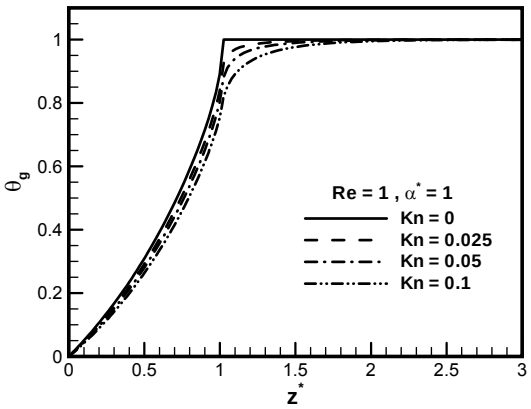

Figure 10. Axial variations of the gas temperature adjacent to walls at Re = 1.

Figure 10 shows the axial variations of gas temperature adjacent to the wall along the channel for various Kn numbers at Re = 1. Solid line corresponding to the no slip case basically shows the peripherally averaged wall temperature, which varies from zero at the inlet to 1 at the end of adiabatic section. Therefore, the difference between the dashed lines and the solid line indicates the peripherally averaged temperature jump at a given location. Temperature jump is directly proportional to Kn and the normal temperature gradients. Apparently, normal temperature gradients are maximum, where velocity slip is maximum (see Figure 6, $z/D \approx 1$) due to the higher convective effects. Temperature jump vanishes as fluid approaches wall temperature along the channel, which seems to occur rather fast at this Reynolds number. Temperature jump is more evident at higher Reynolds number as will be discussed latter.

Figure 10 is also related to the thermal creep effects, since the slope of the dashed lines at each location is directly proportional to the thermal creep contribution to the velocity slip. This figure confirms the finding from Figure 6, which indicates that thermal creep effect is a weak function of Knudsen number.

In general, temperature distribution in the slip-flow regime for a given geometry is governed by Kn and Peclet numbers. Since in the present study, the Prandtl is assumed constant, Reynolds number becomes the influential parameter. In Figure 11, the effect of Reynolds number on the gas temperature is examined. This figure shows the variations of the peripherally averaged gas temperature for different Reynolds numbers, while Knudsen number is fixed, Kn = 0.1. In the

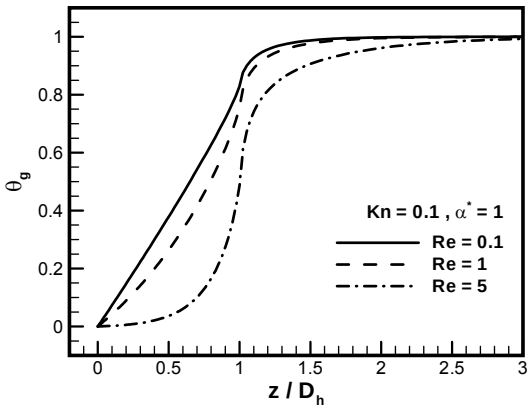

Figure 11. Effect of Re number on axial variations of the gas temperature adjacent to the wall.

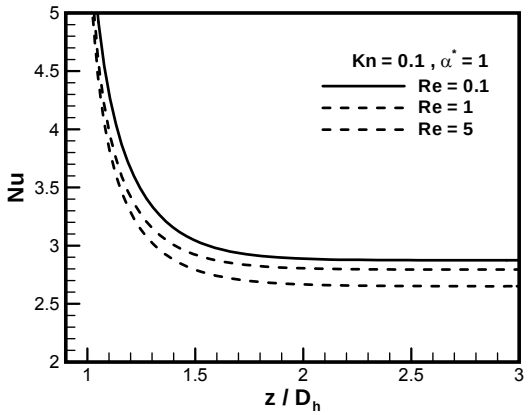

Figure 13. Axial variations of Nu number in a square microchannel at Kn = 0.1 and different Re.

adiabatic section, where convection and conduction occur in the axial direction, as Re increases the convective effects become more dominant and gas temperature is more influenced by upstream effects as is clear for the case with Re = 5. Therefore, for this Re number thermal creep effect is almost zero at the early sections of the channel, while it gains weight when the constant wall temperature is approached. Despite the fact that the axial temperature gradient becomes higher in this region as Reynolds number increases, the relative contribution of thermal creep to the slip velocity decrease dramatically as shown in Figure 5. The relative importance of each component of slip velocity is identified when they are normalized by the mean axial velocity, which increases directly with the Reynolds number for a given geometry. This accounts for the fact that thermal creep effect reduces dramatically with the increase in Reynolds number. Considering the constant wall temperature section, it is clear that the temperature jump increases at higher Reynolds numbers. Temperature jump acts as a contact resistance and reduces the heat transfer rates.

The circumferentially-averaged local heat transfer coefficient along a square microchannel at Re = 1 is plotted in Figure 12. The Nusselt number decreases monotonically in the constant wall temperature section to its fully developed value. Clearly heat transfer rates decrease as Kn number increases due to the increase in temperature jump. The fully developed value of heat transfer rate decreases to about 16% of its no-slip condition value at Kn = 0.1 at this Reynolds number.

In low Reynolds number flows, the heat transfer rate is a function of Reynolds number at a given Prandtl number. In Figure 13, the variations of Nu number along a square channel for various Re numbers at Kn = 0.1 are plotted. As mentioned earlier, temperature jump is more pronounced at higher Re, and therefore, the heat transfer rate is expected to decrease as Re increases in the slip regime. A reduction of about 8% in fully developed Nu number is obtained as Re increases from Re = 0.1 to 5.

Clearly, the fully developed heat transfer coefficients are reduced in the slip regime with an increase in Kn as shown in Figure 14, where the fully developed Nu are plotted as a function of aspect ratio for Re = 1 and different Knudsen numbers. However, this reduction is not expected intuitively, since velocity slip increases the heat transfer rate due to the convective effects, while temperature jump acts as a contact resistance and reduces the heat transfer rate. It seems the temperature jump effect is more dominant and thus the heat transfer rate decreases as the Knudsen number increases. Furthermore, note that as the aspect ratio decreases from the square channel towards the parallel plate limit, the heat transfer rates increase at all Kn as the corner regions lose their influence.

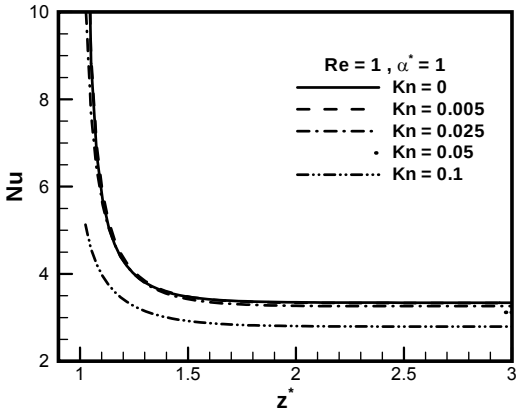

Figure 12. Axial variations of Nu number in a square microchannel at different Kn numbers for Re = 1.

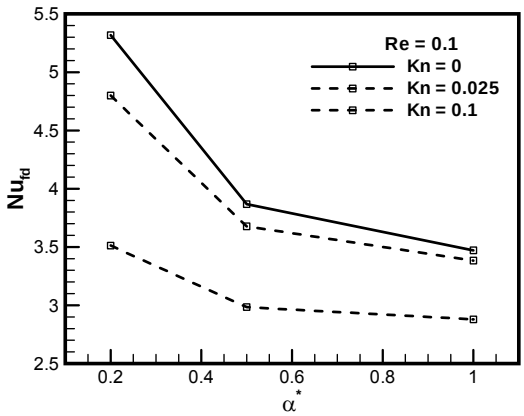

Figure 14. Fully developed heat transfer coefficients as a function of aspect ratio for various Kn numbers.

CONCLUSION

Rarefaction and thermal creep effects on the flow and thermal development from uniform inlet profiles are numerically examined in the slip and continuum flow regimes, Kn ≤ 0.1. Different channel aspect ratios $0.2 \leq \alpha^* \leq 1$ for Reynolds numbers related to microchannels flows in the range of $0.1 \leq Re \leq 5$ with Pr = 1 are considered. Thermal creep effects on the main flow parameters such as friction and heat transfer coefficients are studies for the case of constant wall temperature. An adiabatic entrance section with a length of one D_h is considered such that the constant inlet temperature is more consistent with upstream axial conduction. It is found that the thermal creep effect on velocity slip is stronger at lower Reynolds numbers, where the normal velocity gradient contributions to the velocity slip are weaker. Furthermore, thermal creep effects are slightly affected by Knudsen number, while normal gradient contribution is directly related to the Kn. Both friction and heat transfer coefficients decrease significantly due to the rarefaction effects.

In contrast to the normal velocity gradients contribution to the velocity slip, which approaches a constant value in the fully developed region, thermal creep contribution is mainly in the entrance region and vanishes in the fully developed region.

ACKNOLEDGMENT

The financial support of the Natural Science and Engineering Research Council of Canada (NSERC) and the Ferdowsi University of Mashhad are gratefully acknowledged.

REFERENCES

Bao, F. and Lin, J. (2008): "Burnett simulation of gas flow and heat transfer in micro Poiseuille flow". *International Journal of Heat and Mass Transfer*, Vol. 51, pp. 4139–4144.

Beskok, A. and Karniadakis, G.E. (1992): "Simulation of slip-flows in complex micro geometries". *J. Micromech. Syst. DSC*, Vol. 40, pp. 355-370.

Chen, C and Weng, H.C. (2006): "Developing natural convection with thermal creep in a vertical microchannel". *J. Phys. D: Appl. Phys,* Vol. 39, pp. 3107–3118.

Chorin, A.J. (1968): "Numerical solution of the Navier-Stokes equations". *Math. Comput.*, Vol 22, pp. 745-762.

Dwyer, H.A. (1989): "Calculation of droplet dynamics in high temperature environments". *Prog. Energy Combust. Sci.*, Vol. 15, pp. 131-158.

Ghahremani, A.R., Safari Mohsenabad, S. and Behshad Shafii, M. (2008): "Analytical Solution for Compressible Gas Flow Inside a Two-Dimensional Poiseuille Flow in Microchannels with Constant Heat Flux Including the Creeping Effect." Proceedings of world academy of science, Engineering and technology, Vol. 33, ISSN 2070-3740.

Méolans, J.G. and Graur, I.A. (2008): "Continuum analytical modeling of thermal creep". *European Journal of Mechanics - B/Fluids*, Vol. 27, Issues 6, pp. 785-809.

Niazmand, H., Amiri Jaghargh, A. and Renksizbulut, M. (2009): "Slip-flow and Heat Transfer in Isoflux Rectangular Microchannels with Thermal Creep Effect", Submitted for publication to the *Journal of Applied Fluid Mechanics*.

Niazmand, H., Renksizbulut, M. and Saeedi, E. (2008): "Developing slip-flow and heat transfer in trapezoidal microchannels*", International Journal of Heat and Mass Transfer*. Volume 51, Issues 25-26, pp. 6126-6135.

Renksizbulut, M. and Niazmand, H. (2006): "Laminar flow and heat transfer in the entrance region of trapezoidal channels with constant wall temperature". *J. Heat Transfer*, Vol. 128, pp. 63-74.

Rij, J.V., Harman, T. and Ameel, T. (2007): "The effect of creep flow on two-dimensional isoflux microchannels". *Int. J. Thermal Sciences*, Vol. 46, pp. 1095-1103.

Sazhin, O., Kulev, A., Borisov, S. and Gimelshein, S. (2008): "Numerical analysis of gas-surface scattering effect on thermal transpiration in the free molecular regime". *Vacuum*, Vol. 82, pp. 20-29.

Turner, S.E., Lam, L.C., Faghri, M. and Gregory, O.J. (2004): "Experimental investigation of gas flow in microchannels". *J. Heat Transfer*, Vol. 126, pp. 753-763.

Weng, H.C. and Chen, C (2008): "On the importance of thermal creep in natural convective gas microflow with wall heat fluxes". *J. Phys. D: Appl. Phys.*, Vol. 41, pp.

Wu, P. and Little, W.A. (1983): "Measurements of friction factors for the flow of gases in very fine channels used for micro miniature Joule-Thomson refrigerators". *Cryogenics*, Vol. 23, pp. 273-277.